JOURNAL OF AIRCRAFT
Vol. 36, No. 1, January–February 1999

Response Surface Models Combining Linear and Euler Aerodynamics for Supersonic Transport Design

Duane L. Knill,* Anthony A. Giunta,† Chuck A. Baker,‡ Bernard Grossman,§ William H. Mason,¶
Raphael T. Haftka,** and Layne T. Watson††
Virginia Polytechnic Institute and State University, Blacksburg, Virginia 24061-0203

A method has been developed to efficiently implement supersonic aerodynamic predictions from Euler solutions into a highly constrained, multidisciplinary design optimization of a High-Speed Civil Transport. The method alleviates the large computational burden associated with performing computational fluid dynamics analyses through the use of variable-complexity modeling techniques, response surface (RS) methodologies, and coarse-grained parallel computing. Using information gained from lower-fidelity aerodynamic models, reduced-term RS models representing a correction to the linear theory RS model predictions are constructed using Euler solutions. Studies into 5-, 10-, 15-, and 20-variable design problems show that accurate results can be obtained with the reduced-term models at a fraction of the cost of creating the full-term quadratic RS models. Specifically, a savings of 255 CPU hours out of 392 CPU hours required to create the full-term RS model is obtained for the 20-variable problem on a single 75-MHz IP21 processor of a Silicon Graphics, Inc. *Power Challenge*.

Nomenclature

b	= wingspan
C_D	= drag coefficient
C_{D_0}	= drag polar shape parameter
C_L	= lift coefficient
c_{root}	= root chord
c_{tip}	= tip chord
$\hat{c}_0$, $\hat{c}_j$, $\hat{c}_{jk}$	= response surface model coefficients
$\boldsymbol{g}(\boldsymbol{x})$	= vector of optimization constraint values
K	= drag polar shape parameter
m	= number of design variables
N	= number of points used to evaluate response surface model error
n	= number of terms in the response surface model
n_p	= number of processors used on a parallel computer
p	= number of experimental design points
q	= number of candidate sample sites
R_{LE}	= leading-edge radius parameter
r_{fus_i}	= fuselage radius at ith axial location
s_{LE_I}	= inboard leading-edge length
s_{TE_I}	= inboard trailing-edge length
$(t/c)_{\text{break}}$	= thickness-to-chord ratio at leading-edge break
$(t/c)_{\text{root}}$	= thickness-to-chord ratio at wing root
$(t/c)_{\text{tip}}$	= thickness-to-chord ratio at wing tip
$W_{C\text{-TOGW}}$	= corrected takeoff gross weight
W_{fuel}	= fuel weight
W_{TOGW}	= takeoff gross weight
W_{wing}	= wing weight
$\boldsymbol{x}$	= m-dimensional vector of design variable values
$(x/c)_{\text{max-}t}$	= chordwise location of maximum thickness
x_j	= jth design variable
$\boldsymbol{x}_{\max}$	= vector of upper bounds on design variable values
$\boldsymbol{x}_{\min}$	= vector of lower bounds on design variable values
y	= observed response value
$\hat{y}$	= predicted response value
y_{nac}	= spanwise location of inboard nacelle
ΔC_{D_0}	= correction to linear theory value of the drag polar shape parameter
ΔK	= correction to linear theory value of the drag polar shape parameter
ΔW_{fuel}	= correction to fuel weight
Δy_{nac}	= distance between nacelles
Λ_{LE_I}	= inboard leading-edge sweep angle
Λ_{LE_O}	= outboard leading-edge sweep angle
Λ_{TE_I}	= inboard trailing-edge sweep angle

Received Feb. 1, 1998; revision received June 20, 1998; accepted for publication Aug. 9, 1998.

*Graduate Research Assistant, Multidisciplinary Analysis and Design Center for Advanced Vehicles, Department of Aerospace and Ocean Engineering; currently Postdoctoral Research Associate, Department of Aeronautics and Astronautics, University of Washington, Seattle, WA 98195-2400. Member AIAA.

†Graduate Research Assistant, Multidisciplinary Analysis and Design Center for Advanced Vehicles, Department of Aerospace and Ocean Engineering; currently Postdoctoral Research Associate, National Research Council/NASA Langley Research Center, Hampton, VA 23681. Member AIAA.

‡Graduate Research Assistant, Multidisciplinary Analysis and Design Center for Advanced Vehicles, Department of Aerospace and Ocean Engineering. Student Member AIAA.

§Professor and Department Head of Aerospace and Ocean Engineering, Multidisciplinary Analysis and Design Center for Advanced Vehicles. Associate Fellow AIAA.

¶Professor of Aerospace and Ocean Engineering, Multidisciplinary Analysis and Design Center for Advanced Vehicles. Associate Fellow AIAA.

**Multidisciplinary Analysis and Design Center for Advanced Vehicles; currently Professor of Aerospace Engineering, Mechanics and Engineering Science, University of Florida, Gainesville, FL 32601. Fellow AIAA.

††Professor of Computer Science and Mathematics, Multidisciplinary Analysis and Design Center for Advanced Vehicles.

I. Introduction

WITH advances in computational fluid dynamics (CFD) code maturity, grid-generation capabilities, and computer performance, the application of CFD in aircraft systems design[1] has received much attention. According to Nicolai,[2] about 80% of the aircraft life-cycle cost is set at completion of the conceptual design stage. Using more accurate aerodynamic predictions early in the design process, when the aircraft is initially defined, can result in less time and money spent in redesign and an overall improved product. However,

the relatively large computational expense associated with CFD analyses can discourage its application in design optimization procedures involving more than a small number of variables. A new method must be developed to enable the efficient implementation of accurate CFD predictions into high-dimensional, highly constrained multidisciplinary design optimization (MDO) procedures. This paper presents details and discusses results of such a method as applied to the MDO of a High-Speed Civil Transport (HSCT) (Fig. 1) configuration.

The main component of this method involves utilizing information gained from inexpensive lower-fidelity aerodynamic models to more efficiently create quadratic response surface (RS) models for quantities used to evaluate performance-/aerodynamic-related constraints. While the specific implementation varies, this approach is based on the ideas of variable-complexity modeling (VCM) techniques developed at Virginia Polytechnic Institute and State University (VPI&SU)[3-6] In general terms, VCM combines the accuracy of higher-fidelity results with the computational efficiency of simpler models.

In this research, simple conceptual level models are used to select an appropriate set of intervening functions for which to construct RS models. These RS models are then created using supersonic linear theory aerodynamics. In this paper, linear theory aerodynamics refers to a combination of slender body theory wave drag results, supersonic panel results for the drag due to lift, and a strip boundary-layer correction for the viscous drag. Section III provides details of these analysis methods. Statistical techniques are applied to the linear theory RS models to reveal the terms that have a significant impact on calculating the desired aerodynamic quantities. Terms that have little or no effect can be removed without degrading the accuracy of the RS models. Only the important terms are retained when the reduced-term RS models are constructed using Euler solutions with viscous drag corrections, thereby requiring fewer CFD analyses to compute the coefficients of the models. The reduced-term models are created as corrections to the full-term linear theory RS models. In using such an approach, there is a possibility that the influences of certain important nonlinear effects will be missed. The results will show, however, that this is not the cause for cruise drag predictions of our HSCT designs.

Results obtained from the linear theory RS models are also used to identify the likely neighborhood of the optimal designs from Euler analysis. This enables smaller bounds on each design variable, which improves the accuracy of the RS models.

Coarse-grained parallel computing comprises the final component of the method, enabling efficient computation of the numerous CFD solutions required. Details of the parallel implementation are presented in Appendix A. For consistency, all CPU times presented in this paper are given in terms of single processor performance; however, parallel computation on the 119 node Intel *Paragon* XP/S at VPI&SU reduced the computational times by factors of over 45 with 53 processors. Speedups of this quality are not necessarily obtainable with this coarse-grained approach, as evidenced in parallel applications of structural optimization presented by Balabanov et al.[6] and Burgee et al.[7]

Using VCM techniques, RS methodologies, and coarse-grained parallel computing has enabled the efficient application of accurate CFD analyses into the combined aerodynamic–structural optimization of an HSCT. This method is tested on HSCT design problems of 5, 10, 15, and 20 variables.

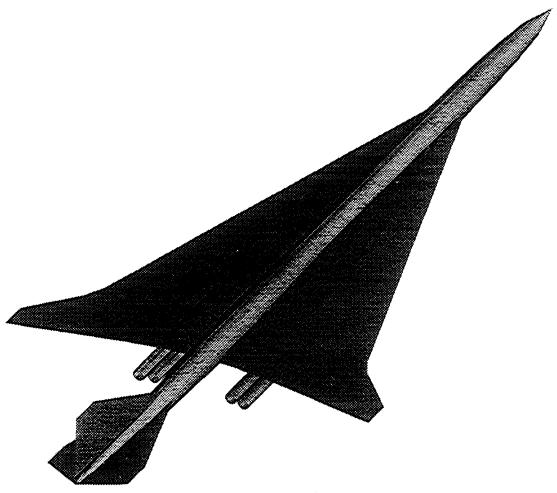

Fig. 1 Typical HSCT configuration.

II. HSCT Design Testbed

The design problem involves minimizing the takeoff gross weight (TOGW) of an HSCT with a 5500-n mile range, designed to cruise at Mach 2.4 and carry 250 passengers. In this study, the aircraft geometry and mission are parameterized by as many as 20 design variables. Figure 2 shows the aircraft development from the set of design variables. The wing planform is created with eight design variables specifying the root chord, tip chord, semispan, inboard leading edge (LE) length, inboard LE sweep angle, outboard LE sweep angle, inboard trailing edge (TE) length, and inboard TE sweep angle. The airfoil sections are described using five design variables: the LE radius parameter, location of maximum thickness, and the thickness-to-chord ratios at the wing root, LE break, and wing tip. The wing thickness is varied linearly between these three spanwise locations. Fuselage radii are specified at four axial restraint locations. The shape of the body between these points is then determined by considering it as a minimum wave drag body of a fixed volume.[3,8] The final variables specify the inboard nacelle placement, the separation between the inboard and outboard nacelles, and the fuel weight. The allowable ranges of values for these variables are shown in Table 1. The vertical tail shape, engine thrust, relative position of the wing to the fuselage, and the cruise climb rate and altitude are fixed.

The optimization uses up to 50 inequality constraints dealing with the aircraft geometry and performance/aerodynamics. These constraints (Table 2) are devised to ensure feasible aircraft geometries and impose realistic performance and control capabilities. Fuel volume and wing chord length limits are examples of geometric constraints. Performance/aerodynamic constraints include, for example, landing angle-of-attack limits and wing, tail, and engine scrape prevention criteria. Emergency conditions are used to enforce the landing constraints. It is assumed that the aircraft lands on a runway 5000 ft above sea level at 145 kn, carrying 50% of its initial fuel weight. These are complicated, nonlinear constraints that require aerodynamic forces and moments, stability and control derivatives, and center of gravity and inertia estimates.

An example of the complicated constraint boundaries present in the design spaces associated with this HSCT optimization is shown in Fig. 3. This figure represents a plane in 10-dimensional design space, passing through three design points. Two of the design points represent local optima found by the optimizer, and the third point is a suboptimal feasible point. The design points represented by the open circles are feasible points, whereas those represented by the filled circles have violated some constraints. The plot illustrates the nonconvexity of the design space caused by the aerodynamic constraints. If the optimizer drives the design near optimum 1, it cannot cross the boundary created by the range constraint to arrive at optimum 2, which is 2000 lb lighter. Clearly, using RS models does not eliminate the problem of local optima. In this work we have dealt with this difficulty by using multiple starting points to locate the best local optimum. Performing a number of optimizations using the polynomial approximations is relatively inexpensive. The bulk of the computational time is spent up front on creating the RS models. Methods for global optimization may be more effective for dealing with the local op-

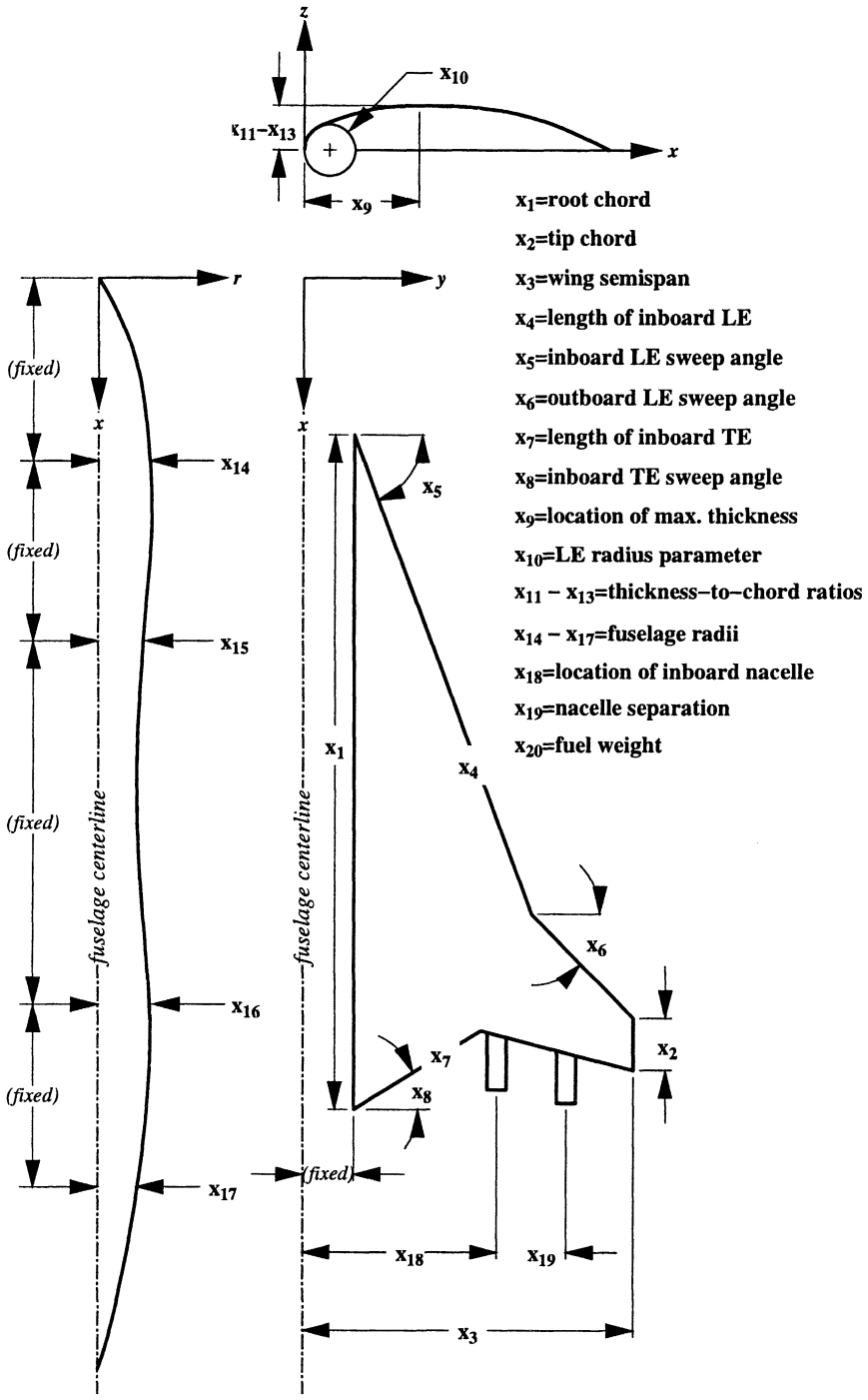

Fig. 2 Definition of the 20 design variables.

tima problem. We are now considering several global optimization methods for this purpose.

A series of optimization problems of 5, 10, 15, and 20 variables serve to evaluate our methods of including Euler analyses in multidisciplinary HSCT design. The design variables (Table 1) and constraints (Table 2) for the simplified problems are subsets of those used in the 20-variable design. The upper and lower limits of the active design variables remain the same throughout the series of optimization problems. These bounds on the design variables are selected from optimization results performed using the linear theory RS models. For the 5-, 10-, and 15-variable problems we can afford the evaluations required to create full-term quadratic RS models, providing us with a means to assess the performance of the reduced-term models.

III. HSCT Design Tools

A. Linear Theory Aerodynamics

What we term supersonic linear theory predictions are actually obtained from three codes, each computing a particular component of the drag. The volumetric wave drag is computed using the Harris[9] wave drag program. Drag due to lift is calculated using a panel method by Carlson and Miller,[10] with attainable LE thrust corrections.[11] Viscous drag estimates are obtained using standard algebraic estimates[12] of the skin friction assuming turbulent flow. These viscous drag predictions are also added to the Euler solution.

Wing camber for the HSCT designs is determined using a linear theory code with empirical corrections to account for nonlinear effects named WINGDES.[10,13] WINGDES attempts

Table 1 Design variable limits in the optimization problems

Variable	Number of variables 5	10	15	20
		Planform variables		
c_{root}, ft	150–190	150–190	150–190	150–190
c_{tip}, ft	7–13	7–13	7–13	7–13
$b/2$, ft	[74]	58–78	58–78	58–78
s_{LE_I}, ft	[132]	[132]	105–135	105–135
Λ_{LE_I}, deg	67–76	67–76	67–76	67–76
Λ_{LE_O}, deg	[25]	12–32	12–32	12–32
s_{TE_I}	Straight TE	Straight TE	Straight TE	10–30 ft
Λ_{TE_I}	Straight TE	Straight TE	Straight TE	−55–16 deg
		Airfoil variables		
$(x/c)_{max\text{-}t}$, %	[40]	38–52	38–52	38–52
R_{LE}	[2.5]	2.1–4.1	2.1–4.1	2.1–4.1
$(t/c)_{root}$, %	1.5–2.7	1.5–2.7	1.5–2.7	1.5–2.7
$(t/c)_{break}$	$(t/c)_{break} = (t/c)_{root}$	$(t/c)_{break} = (t/c)_{root}$	$(t/c)_{break} = (t/c)_{root}$	1.5–2.7%
$(t/c)_{tip}$	$(t/c)_{tip} = (t/c)_{root}$	$(t/c)_{tip} = (t/c)_{root}$	$(t/c)_{tip} = (t/c)_{root}$	1.5–2.7%
		Fuselage variables		
r_{fus_1}, ft	[5.2]	[5.2]	4.5–6.0	4.5–6.0
r_{fus_2}, ft	[5.7]	[5.7]	4.5–6.0	4.5–6.0
r_{fus_3}, ft	[5.9]	[5.9]	4.5–6.0	4.5–6.0
r_{fus_4}, ft	[5.5]	[5.5]	4.5–6.0	4.5–6.0
		Nacelle and mission variables		
y_{nac}, ft	[20]	10–35	10–35	10–35
Δy_{nac}, ft	[6]	[6]	[6]	6–18
W_{fuel}	No limits	No limits	No limits	No limits

Note: [ ] indicates variable value when not active in the design.

Table 2 Constraints applied in the optimization problems

Number	Constraint	Number of variables 5	10	15	20
1	Range ≥ 5500 n mile	X	X	X	X
2	C_L at landing speed	X	X	X	X
3–20	Section $C_l \leq 2$	X	X	X	X
21	Landing $\alpha \leq 12$ deg		X	X	X
22	Fuel volume	X	X	X	X
23	Spike prevention	X	X	X	X
24–41	Wing chord ≥ 7.0 ft	X	X	X	X
42, 43	Engine scrape		X	X	X
44, 45	Engine scrape (5-deg roll)		X	X	X
46	Wing-tip scrape		X	X	X
47	TE break scrape (5-deg roll)		X	X	X
48	LE break ≤ semispan	X	X	X	X
49	TE break ≤ semispan				X
50	Engine-out limit (vertical tail design)	X	X	X	X
		42[a]	49[a]	49[a]	50[a]

[a]Number of applied constraints.

to find the camber distribution along the wing that minimizes the drag caused by lift. Two runs of WINGDES per design were required to get the proper camber distribution. The second run serves to smooth the camber distribution and provide the maximum leading-edge suction parameter at the design lift coefficient.

B. Computational Fluid Dynamics

Version 2.2 of the General Aerodynamic Simulation Program[14] (GASP) is used to obtain the Euler solutions. GASP is a fully conservative CFD code that solves the Reynolds-averaged Navier–Stokes equations and many of its subsets. The code uses an upwind three-dimensional finite volume spatial discretization and, for our calculations, a third-order upwind-biased interpolation of the Roe fluxes is used in each of the marching planes. Space marching has been performed for all of the CFD calculations. The accuracy of the CFD predictions has been studied extensively by Knill et al.[15] These studies confirmed that the Euler drag results are accurate within 1/2 count ($\Delta C_D = 1.0 \times 10^{-4}$ corresponds to 1 count of drag), in the range of flight conditions considered using 405,000 grid cells.

Grids suitable for space-marching calculations on the HSCT wing–fuselage configurations are created using a grid generator originally developed by Barger.[16] The code was modified[17] to provide better resolution of the LE and remain robust for large changes in the aircraft geometry. The grid generator receives as input the aircraft configuration stored in the Craidon[18] geometry format, extends the wing to join the fuselage, performs filleting of the wing–fuselage intersection,[19] and then creates a grid for space-marching calculations. Two marching planes for a wing–fuselage configuration are shown in Fig. 4. Because our HSCT optimization code creates a Craidon description file from its set of design variables, the conversion from a set of design variables to a space-marching CFD grid is straightforward. The grid generator is automated and robust for large planform changes, essential qualities for application in design optimization.

C. Weight Estimation

All components of the TOGW are calculated using empirically based functions obtained from the Flight Optimization System[20] (FLOPS) weight equations.

D. Optimization Routine

Optimization is performed using the software package Design Optimization Tools[21] (DOT). The constrained optimization is performed using sequential quadratic programming and central-difference gradient approximations. The optimization problem is the minimization of the TOGW subject to a number of constraints related to both the geometry and the mission.

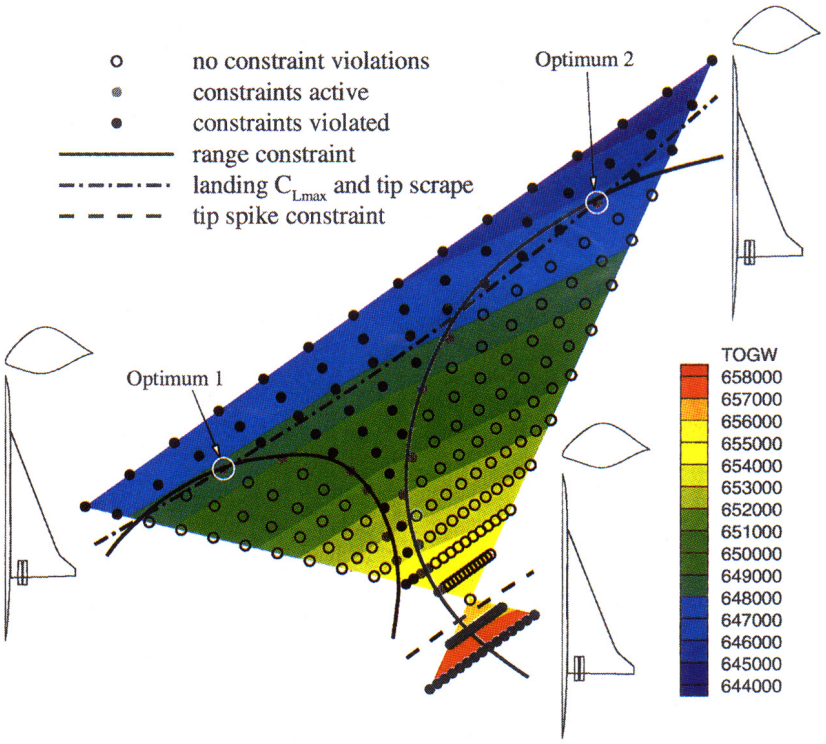

Fig. 3 Nonconvex design space in a 10-variable problem.

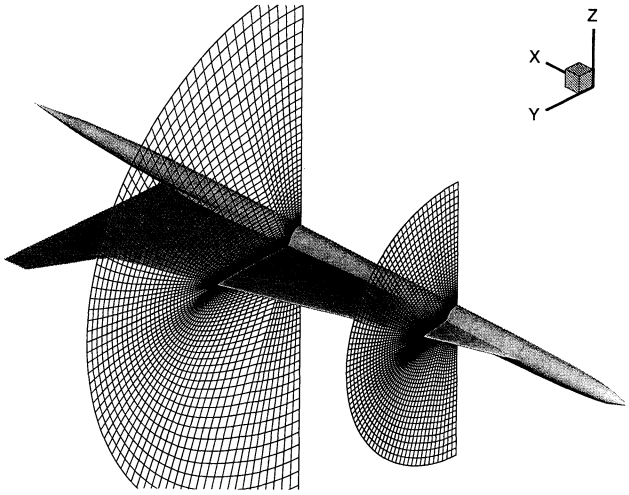

Fig. 4 HSCT with CFD grid planes.

Side constraints limit the values of the design variables. The optimization problem can be written as

$$\min_{x \in \mathcal{R}^m} \text{TOGW}(\boldsymbol{x})$$

subject to

$$\boldsymbol{g}(\boldsymbol{x}) \leq 0, \qquad \boldsymbol{x}_{\min} \leq \boldsymbol{x} \leq \boldsymbol{x}_{\max} \tag{1}$$

IV. RS Modeling

To use relatively expensive Euler solutions for the large number of constraint evaluations required in our multidisciplinary optimization, RS models of the supersonic aerodynamics are created. RS modeling techniques have been used for a number of years to solve complex, computationally intensive engineering problems. In 1964, Powers[22] applied this technique to find minimum drag bodies of revolution using results from a real-gas blunt-body program and a real-gas method of characteristics program. RS modeling techniques for aerodynamic and structural design improve the performance of highly constrained gradient-based optimizations.[6,23–25] The RS models smooth out numerical noise present in the analyses. Numerical noise manifests itself as low-amplitude, high-frequency noise present in the analyses. Numerical noise manifests itself as low-amplitude, high-frequency variations in the computational results with changes in the design variables. These variations are present in any method with iterative procedures or discrete representations of continuous geometric shapes or physical phenomena.[26,27] This noise distorts gradient information and can lead to artificial local minima in the design space. In addition, the analysis codes are separated from the optimization routines, eliminating the need to integrate large, production-level grid generators, analysis codes, and postprocessing utilities with the optimizer. This also allows analyses to be performed by experts in the specific discipline on parallel architecture machines. Finally, by replacing complex analysis codes with simple quadratic polynomials, one can readily obtain information on design tradeoffs, sensitivities to certain variables, and insight into the highly constrained, nonconvex design spaces. Details of tradeoff studies are presented in Appendix B.

A. Functional Form of the Response

Not all response functions can be modeled accurately by low-order polynomials, but often accuracy can be improved by transformations of the function or its arguments. Analytic solutions obtained under simplifying assumptions often help reveal the needed transformations. The use of such transformations was pioneered for approximations of structural response by Schmit and Vanderplaats and their coworkers (see Ref. 28). They called the transformed variables and functions "intervening variables" and "intervening functions," respectively.

Our group has made use of intervening variables to improve the accuracy of the RS model for optimal structural weight as a function of the HSCT configuration variables.[5] Golovidov[29] showed that approximating the drag coefficient by a quadratic polynomial and calculating the range from the drag coefficient improves the accuracy over direct approximation of the range. The drag coefficient became the intervening function for the range.

In the present work, we use the knowledge that for uncambered wings, the drag coefficient is approximately a simple quadratic function of the lift coefficient, written as

$$C_D(\boldsymbol{x}) = C_{D_0}(\boldsymbol{x}) + K(\boldsymbol{x})C_L^2 \tag{2}$$

We then fit the intervening functions, $C_{D_0}(\boldsymbol{x})$ and $K(\boldsymbol{x})$, by quadratic RS models. Using this form has the added advantage of removing the dependence of the drag coefficient on the fuel weight, introduced only through the lift coefficient.

The HSCT wings have little camber because they are optimized for cruise at Mach 2.4; therefore, this form of the drag polar for uncambered wings is still fairly accurate. The error in fitting the Euler drag polars to this form is less than 0.5 count over $0.05 \leq C_L \leq 0.12$. These values of C_L cover the range of cruise lift coefficients found for our HSCT designs.

B. Creating Quadratic RS Models

A quadratic RS model in m variables has the form

$$\hat{y} = \hat{c}_0 + \sum_{1 \leq j \leq m} \hat{c}_j x_j + \sum_{1 \leq j \leq k \leq m} \hat{c}_{jk} x_j x_k \tag{3}$$

There are $(m + 1)(m + 2)/2$ coefficients for a quadratic RS model in m variables. Giunta et al.[30] found that using approximately twice as many points as the number of coefficients is sufficient to accurately compute the value of the coefficients for our low-dimensional HSCT design problems. However, as the dimension of the problem increases, the ratio of the required number of points to the number of terms p/n in the RS also increases.[5] We use a systematic increase from $p/n = 2.0$ in the five variable case to $p/n = 3.5$ in the 20-variable case to provide adequate accuracy. This translates to 60, 276, 720, and 1470 CFD evaluations per RS model for the 5-, 10-, 15-, and 20-variable problems, respectively. While suitable for our HSCT design problems, these requirements on the number of design points are, in general, problem dependent.

To compute the coefficients for the quadratic RS models of both $C_{D_0}(\boldsymbol{x})$ and $K(\boldsymbol{x})$ for a 30-variable problem would require 4184 CFD evaluations. On a single processor of the SGI *Power Challenge*, this would require over 46 days of computation. Clearly, a method must be developed that enables accurate RS estimates with a reduced number of required CFD analyses.

Design of experiments theory provides a systematic means of selecting the set of points (called an experimental design) within the m-dimensional design space. The number of points in this initial screening experimental design is reduced by applying geometric constraints. Using the remaining set of geometrically feasible points, the D-optimality criterion[31] is applied to select the points used in creating the RS models. Appendix C provides further details on the experimental designs used.

C. Reduced-Term RS Models

Linear theory RS models can be readily created for moderately high-dimensional spaces because the evaluations are computationally inexpensive. Stepwise regression analysis provides a means of systematically removing terms from the RS models that have little or no impact on the response. Terms are eliminated using a measure of the significance level of the term called the p value. This represents the probability that the coefficient of a particular term is actually zero, not the value computed. Typically, a p value of 0.05 or less indicates that the term is significant in predicting the variation in the response. As the prescribed value of the p value is reduced, more terms are eliminated from the RS model. At some point in the stepwise regression process, the error in the RS model fit increases noticeably, indicating that too many terms have been eliminated to satisfy the p-value limit. For this research, JMP[32] is used to perform the stepwise regression analysis.

The stepwise regression technique is applied to the RS models for the linear theory aerodynamics to create reduced-term RS models. Because the Mach 2.4 cruise regime is predominantly linear, performing stepwise regression analysis on the RS models for the linear theory aerodynamics should give polynomials with the terms that are also important with respect to Euler aerodynamics. Instead of creating full-term quadratic RS models for the Euler results, one needs only to create the reduced-term models found using linear theory analyses. Computational time is therefore not wasted evaluating coefficients that do not have a significant effect on the response.

The rms error estimate is used to indicate the error in the RS model fit. The rms error is calculated as

$$\text{rms error} = \sqrt{\left[\sum_{i=1}^{N} (y_i - \hat{y}_i)^2\right] \Big/ N} \tag{4}$$

The N sample points are a randomly selected subset of the points used in the initial screening experimental design, not including the design points used in the RS model creation.

We have found that the best means to implement the reduced-term RS models with Euler analyses is by using an incremental form (see Ref. 17 for details on other alternatives). This approach uses reduced-term RS models for the difference between the Euler and linear theory RS model predictions of the drag polar shape parameters, $\Delta C_{D_0}(\boldsymbol{x})$ and $\Delta K(\boldsymbol{x})$. To estimate the Euler values of the response, these correction RS models are added to the full-term quadratic linear theory RS models. The sum of the linear theory and correction RS models will be referred to as the incremental RS models, i.e., n-term incremental RS model = n-term correction RS model + full-term linear theory RS model.

V. Optimization Results

Results from stepwise regression analysis for the five variable design are shown in Fig. 5. The rms error in the linear theory RS models represents the differences between the linear theory RS model prediction of the cruise drag and the linear theory analysis value. The rms error in the incremental RS models represents the differences between the incremental RS model prediction of the cruise drag and the actual Euler value. Both errors are computed at 30 points randomly selected from the set of feasible design points not used in the RS model creation. The plot shows that the rms error for the incremental RS model does not have the abrupt increase below seven terms that is present in the linear theory RS models.

The stepwise regression plot demonstrates that the stepwise regression technique can eliminate unimportant terms from the RS models with little or no effect on the error. Furthermore, it shows that the errors in the reduced-term incremental RS models, created using terms found from stepwise regression analysis on the linear theory RS models, do not change significantly as the number of terms is reduced. This indicates

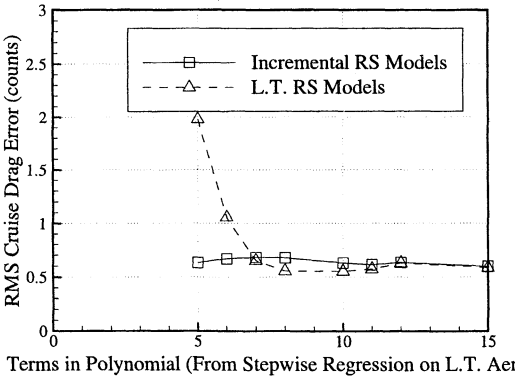

Fig. 5 Stepwise regression (5-variable problem).

that linear theory analysis does reveal the terms that are important to the Euler analyses and that no important nonlinear effects have been masked. The five-term incremental RS models, which require only 10 design points to be evaluated, are chosen to perform the five variable optimization studies.

The five-term incremental RS model requires only 5.3 h to create, compared with 16 h required for the full-term model. The optimal design obtained from the incremental RS models (Fig. 6) compares well with the full-term Euler RS model. The top half of this figure contains the optimal designs for the five variable problem. More importantly, Euler analysis on the optimal design reveals that the RS model cruise drag prediction is less than 0.1 count higher than the Euler value. The design variable values (Table 3) for the incremental RS model optimum fall within their prescribed bounds, demonstrating the success of selecting these bounds based on the linear theory optimal designs. Table 4 shows that the corrected TOGW ($W_{C\text{-}TOGW}$) of 622,500 lb is only 700 lb higher than that for the full-term Euler optimum. The corrected TOGW is the result of adding or subtracting fuel weight (ΔW_{fuel}) to the optimal designs to correct for the range discrepancy caused by differences between the RS model and actual Euler predictions.

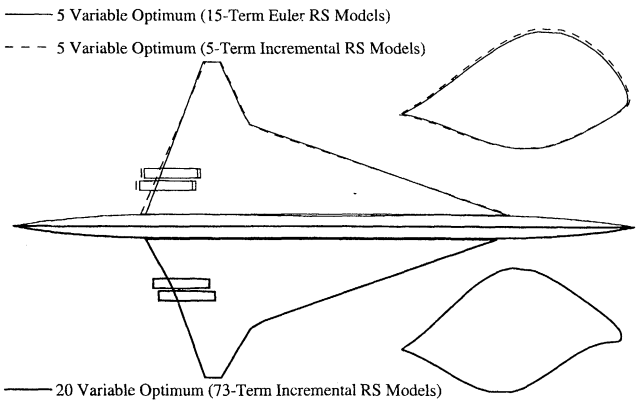

Fig. 6 Optimal configurations from the 5- and 20-variable design problems.

For the 10- and 15-variable designs, using the reduced-term incremental RS models results in savings of 47 out of 74 h and 115 out of 192 h required to create the full-term RS models, respectively. The error in RS model drag prediction for both cases is within 0.6 counts of the value from Euler analysis. The optimal design variable values and weights are given in Tables 3 and 4. Further details of these cases are presented by Knill et al.[33]

Because of computational expense, the full quadratic Euler RS models are not created for the 20-variable design. This is exactly the situation for which the reduced-term incremental RS models were developed. Regression analysis on the linear theory data (Fig. 7) shows that the rms cruise drag error remains nearly constant until about 73 of the original 210 terms remain in the RS models. Creating the 73-term RS models requires data from 256 of the 735 total experimental design points. Euler evaluations for 350 design points were performed to create the 100-term incremental RS models. Because the full-term Euler RS models are not present, this provides a model with which to compare the errors in the 73-term RS models. It is seen that there is no major difference in the cruise drag errors of the 100- and 73-term incremental RS models.

The optimal design from the incremental RS models is shown in Fig. 6 to provide comparison with the five-variable optima. Table 3 provides the optimal design variable values. The cruise drag prediction for the optimal design from the incremental RS models is 0.8 counts lower than the actual Euler value, which is much better than the rms error estimate of the RS models. Compensating for the range deficiency gives a corrected TOGW of 588,000 lb. Table 4 shows the consistent reduction in the optimal wing weight, fuel weight, and TOGW with increasing number of design variables.

Table 3 Design variable values for the optimal designs from incremental RS models

	Number of variables			
Variable	5	10	15	20
		Planform variables		
c_{root}, ft	178.0	170.4	166.2	169.5
c_{tip}, ft	7.4	9.0	7.7	7.8
$b/2$, ft	[74.0]	72.1	68.1	67.4
s_{LE_i}, ft	[132.0]	[132.0]	120.4	124.8
Λ_{LE_i}, deg	71.1	70.0	69.4	70.5
Λ_{LE_o}, deg	[25.0]	18.7	24.2	30.4
s_{TE_i}, ft	Straight TE	Straight TE	Straight TE	27.4
Λ_{TE_i}, deg	Straight TE	Straight TE	Straight TE	−29.0
		Airfoil variables		
$(x/c)_{max\text{-}t}$, %	[40.0]	50.2	49.8	51.1
R_{LE}	[2.5]	2.1	2.1	2.1
$(t/c)_{root}$, %	1.81	1.91	1.99	1.99
$(t/c)_{break}$	$(t/c)_{break} = (t/c)_{root}$	$(t/c)_{break} = (t/c)_{root}$	$(t/c)_{break} = (t/c)_{root}$	1.91%
$(t/c)_{tip}$	$(t/c)_{tip} = (t/c)_{root}$	$(t/c)_{tip} = (t/c)_{root}$	$(t/c)_{tip} = (t/c)_{root}$	1.94%
		Fuselage variables		
r_{fus_1}, ft	[5.2]	[5.2]	5.2	5.2
r_{fus_2}, ft	[5.7]	[5.7]	5.6	5.6
r_{fus_3}, ft	[5.9]	[5.9]	5.6	5.6
r_{fus_4}, ft	[5.5]	[5.5]	5.2	5.2
		Nacelle and mission variables		
y_{nac}, ft	[20.0]	30.0	28.1	27.7
Δy_{nac}, ft	[6.0]	[6.0]	[6.0]	6.0
W_{fuel}, lb	309,800	306,000	299,600	293,300

Note: [ ] indicates variable value when not active in the design.

Using the reduced-term incremental RS models provides a means to create RS models for high-dimensional problems, where computing the coefficients of the full quadratic RS models is not viable. Figure 8 shows how the present model extrapolates to 25 and 30 design variables. The trend indicates that a reduced-term RS model in 25 design variables can be created using the same number of terms as a full quadratic model in 15 design variables.

The rms error estimates for the incremental RS models are consistently higher than the errors in the optimal designs. Investigation led to the finding that the incremental RS model fit through the interior of the design bounding box is better than that at the vertices, where the points used to evaluate the rms errors are located. When evaluating the rms error in the 15-variable design, using a new set of 162 design points scattered through the interior of the design box, the rms error estimate dropped from 1.5 counts to 0.9 count. This indicates that computing the rms errors based solely on points selected from the vertices of the design box may not provide a sufficiently accurate representation of the RS model fit.

The rms errors in the linear theory and incremental RS models steadily increase from the 5-variable through the 20-variable problem. The inability to perform calculations at all vertices of the design bounding box and the nonquadratic behavior of the responses are contributing factors. Preliminary examinations of three methods to improve the accuracy of the RS models have been made. The first method involves using a more accurate physical model to provide the functional form for the drag polar. With an additional CFD evaluation per design, a more accurate cambered form of the drag polar, $C_D(\boldsymbol{x}) = C_{D_m}(\boldsymbol{x}) + K(\boldsymbol{x})[C_L - C_{L_m}(\boldsymbol{x})]^2$, can be evaluated. This approach was found to reduce the rms error in the RS models by approximately 0.3 drag count. The nonquadratic nature of the response can be addressed in two ways: reducing the size of the design bounding box and including cubic terms in the RS model. Reducing the size of the design box has a significant effect on the error; however, care must be taken to ensure that the optimal design lies within the reduced box. Including cubic terms allows one to maintain the size of the original box, but the computational expense of evaluating all of the cubic terms makes it unattractive for high-dimensional problems. Using the more accurate drag polar representation along with a zooming technique to reduce the size of the design box appears to be a promising approach. Research is currently under way to further investigate the merits of these approaches.

Table 4 Weights for optimal designs from full-term and reduced term RS models

	Number of variables			
	5	10	15	20
Reduced-term incremental RS models				
W_{wing}	103,900	96,100	87,800	86,900
W_{fuel}	309,800	306,000	299,600	293,300
W_{TOGW}	622,800	610,400	590,700	583,200
Range:				
(Euler)	5503	5542	5495	5449
ΔW_{fuel}	−320	−3720	450	4430
$W_{C\text{-TOGW}}$	622,500	606,300	591,200	588,000
Full-term Euler RS models				
W_{wing}	103,900	99,200	87,900	—
W_{fuel}	313,200	301,000	300,100	—
W_{TOGW}	626,300	608,900	591,500	—
Range:				
(Euler)	5544	5485	5505	—
ΔW_{fuel}	−4010	1300	−440	—
$W_{C\text{-TOGW}}$	621,800	610,300	591,000	—

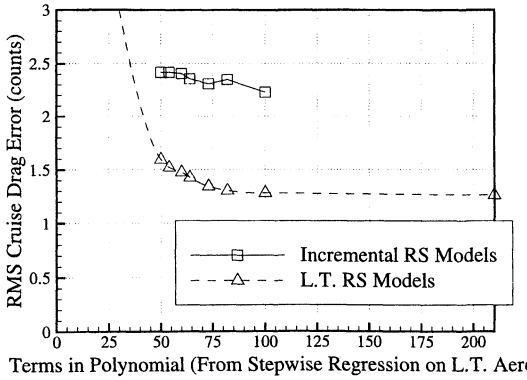

Fig. 7 Stepwise regression (20-variable problem).

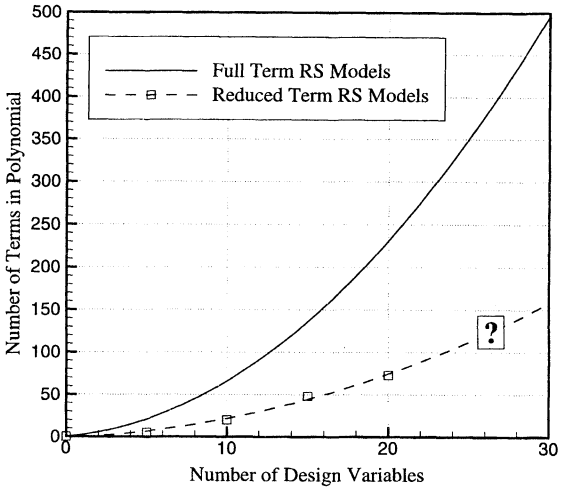

Fig. 8 Number of terms in RS models.

VI. Conclusions

A method for efficiently implementing supersonic Euler analyses in an MDO involving aerodynamics, weights, and performance of an HSCT has been developed and tested on problems of 5, 10, 15, and 20 design variables. This method takes advantage of information obtained from inexpensive lower-fidelity aerodynamic analyses to more effectively create RS models for the Euler solutions. The functional form of the drag polar is selected based on conceptual level aerodynamic models. Correction RS models representing the difference between linear theory and Euler values of the intervening functions, $\Delta C_{D_0}(\boldsymbol{x})$ and $\Delta K(\boldsymbol{x})$, are then created. Incremental RS models for the Euler predictions are then created by adding the correction RS models to the full quadratic linear theory RS models. Optimization results from the linear theory RS models are used to select the design bounding box within which the optimum from Euler analysis should lie. This improves the accuracy of the RS models by allowing smaller ranges on the design variables compared to those required if no information was available on the general location of the optimal design.

Computational expense is reduced using stepwise regression analysis results gained from linear theory analysis to remove terms from the RS models that are not important to the Euler aerodynamics. Compared with the cost of creating full-term RS models, creating the reduced term RS models results in savings of 11 out of 16 h, 47 out of 74 h, 115 out of 192 h, and 255 out of 392 h of CPU time on a single 75-MHz IP21 processor of an SGI *Power Challenge* for the 5-, 10-, 15-, and 20-variable design problems, respectively. Errors in the reduced-term incremental RS model cruise drag predictions, based on actual Euler calculations, for the optimal designs range from 0.1 to 0.8 counts.

Appendix A: Parallel Computing

Over 1000 CFD drag solutions are used to create the RS models and evaluate the errors for the 15- and 20-variable

designs. Performing these calculations on a single processor of the SGI *Power Challenge* R8000 machine would take nearly 2 weeks of wall clock time. This time can be reduced significantly by taking advantage of parallel computing.

A coarse-grained parallelization of the CFD analyses has been implemented on the 119-node, distributed memory Intel *Paragon* XP/S at VPI&SU. While fine-grained parallelization offers potentially better performance, especially for large numbers of nodes, coarse-grained parallelization is easier to implement and does not require in-depth knowledge of or modifications to the complex codes used. The parallel computations are organized in a master-slave paradigm, where one processor creates the directory structure and input files, distributes the jobs, and checks for their completion. Each individual CFD calculation is performed entirely by a single slave node.

Two measures of parallel performance are presented: the parallel speedup and efficiency. Speedup represents the ratio of the serial calculation time to the parallel computation time on n_p nodes. The parallel efficiency is the speedup divided by the number of nodes. Ideally, the speedup equals the number of nodes, bringing the efficiency to 1.0; however, this ideal behavior is not realized. File I/O, which is inherently serial, increases with n_p and prevents the user from approaching ideal speedup and efficiency for large numbers of nodes. Reading and writing of input files, CFD grid files, and CFD solution files are examples of the file I/O present in the procedure.

Despite these detractors, good performance is achieved when implementing the CFD calculations in parallel. Figure A1 shows the parallel speedup and efficiency obtained from performing 1080 CFD calculations for 360 HSCT configurations used in the 15-variable design. When using 27 nodes, a speedup of 24.3 (0.90 efficiency) is realized. When using 53 nodes, a speedup of 45.4 (0.86 efficiency) is achieved. Even though a single processor of the Intel *Paragon* is about 10 times slower than a single processor of the SGI *Power Challenge*, significant improvements in the turnaround time are achieved when using a large number of nodes. On 53 nodes, the 1080 Euler calculations require only 2.8 days to complete.

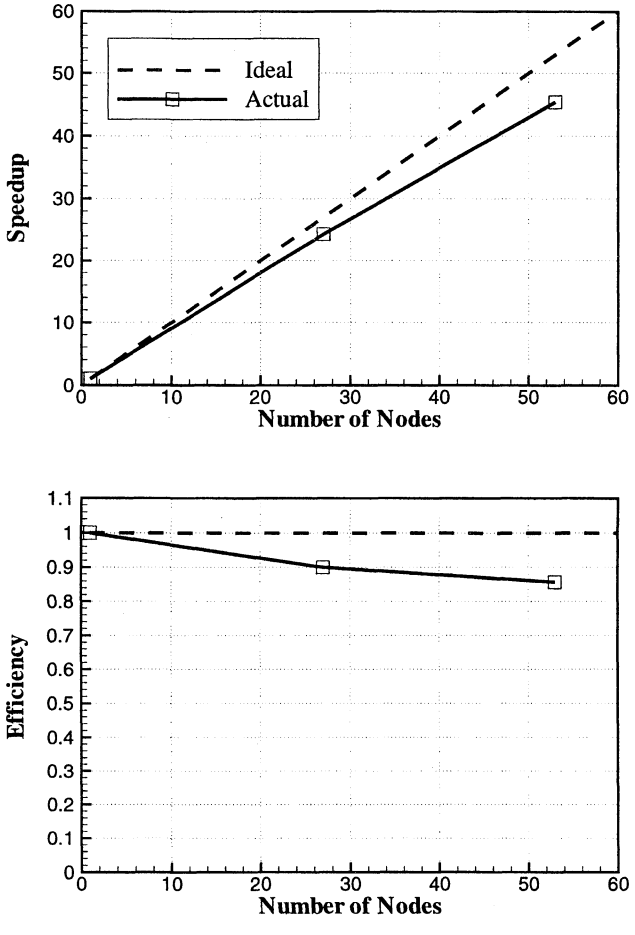

Fig. A1 Parallel speedup and efficiency.

Appendix B: Design Tradeoffs

Parametric studies are invaluable to a designer. These studies provide information on tradeoffs between various disciplines and influences, sensitivities to variations in design variables, and effects of perturbations to a chosen design. To perform a single parametric study, 25–50 analyses may be required. To

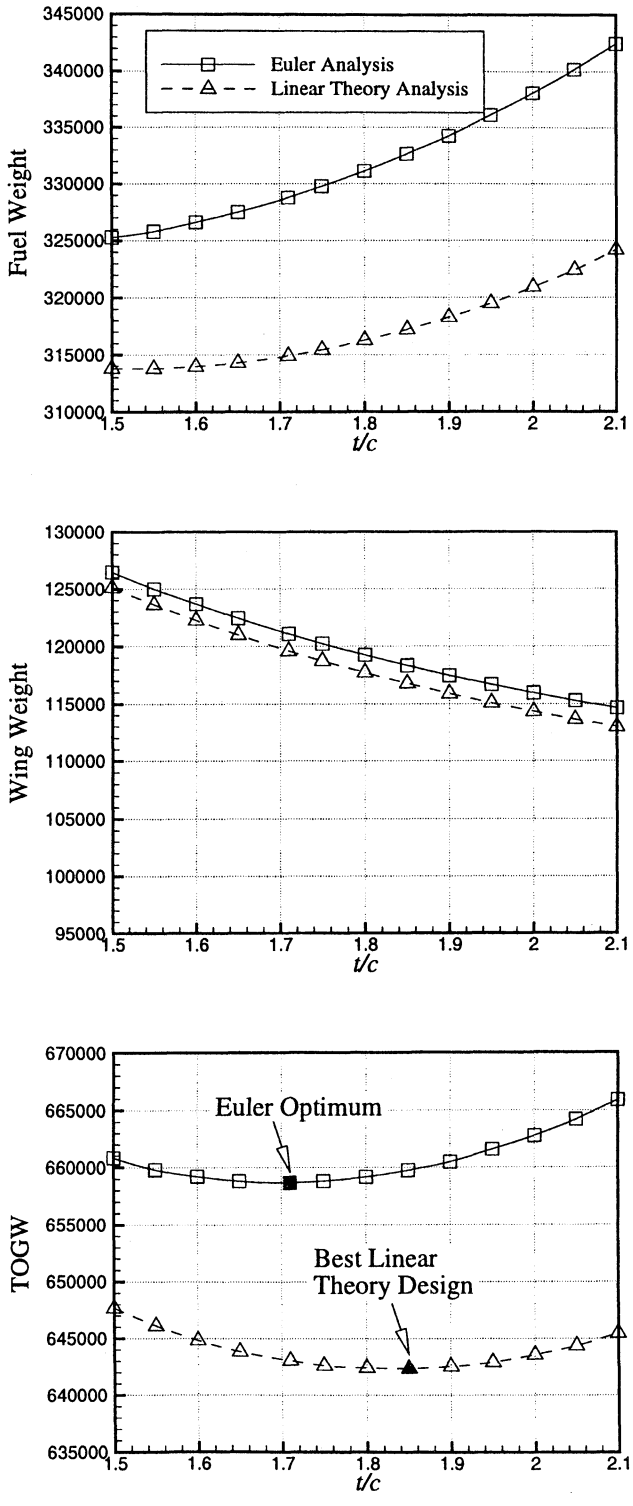

Fig. B1 Aerodynamic–structural tradeoff for *t/c*.

completely examine a design, many of these parametric studies would be desired. The computational burden involved in performing these studies is greatly reduced by using results from RS models instead of data from a large number of CFD calculations, because the expense lies only in the evaluation of the simple quadratic polynomials. In this section, we examine variations in selected design variables to gain insight into the behavior and relative importance of these parameters.

The optimal designs predicted from linear theory and Euler RS models for the 5-, 10-, and 15-variable design problems show the effects of the higher drag predictions typical of the supersonic Euler solutions. The wing thickness is a direct tradeoff (Fig. B1) between aerodynamics and structures. Aerodynamics dictates that the wing should be as thin as possible to reduce the drag, and therefore, the fuel weight. Structural optimization, on the other hand, would attempt to increase the wing thickness to reduce the wing weight. A compromise is met between the fuel and wing weight to obtain the minimum TOGW. The effects of replacing the linear theory aerodynamics with Euler solutions are apparent in the fuel weight. The higher drag predicted from Euler analysis translates to higher fuel weights and a design in which the aerodynamic aspects are more dominant. The optimal design is obtained at a lower t/c value to counter the effects of the higher drag at the expense of the wing weight.

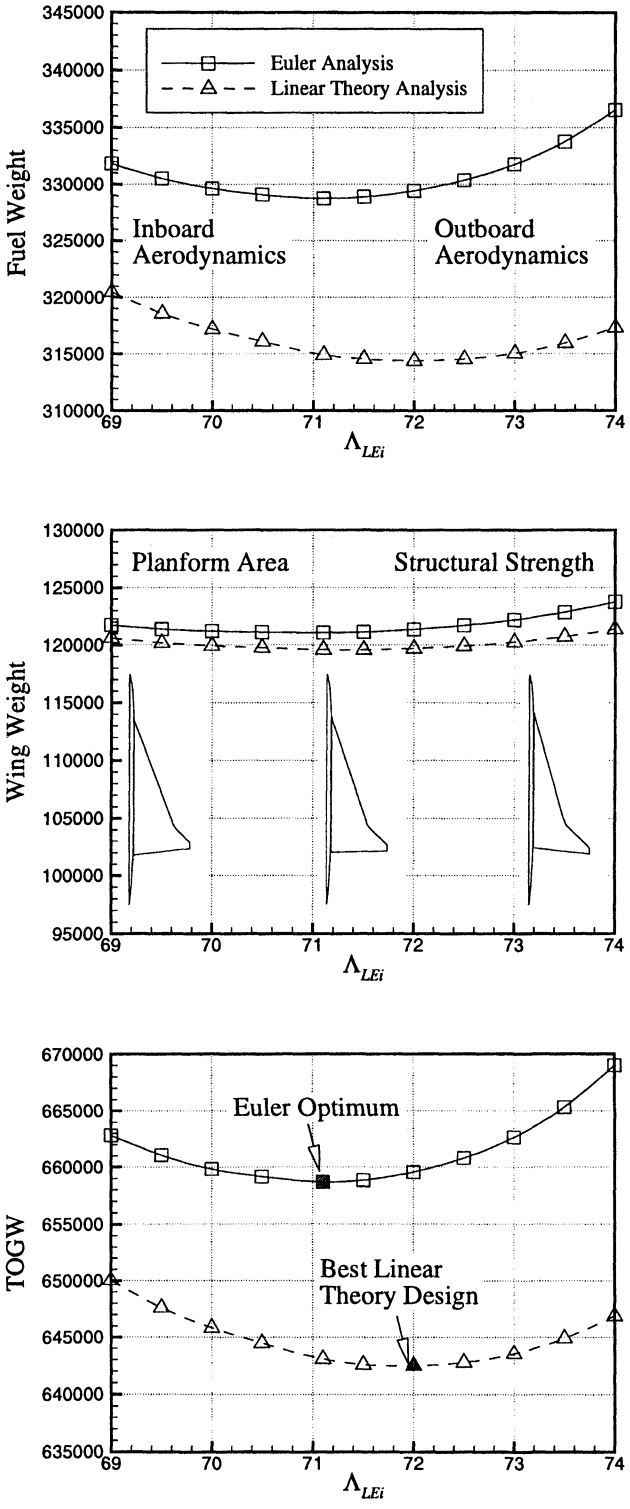

Fig. B2 Tradeoff study for Λ_{LE_i}.

The linear theory curve for the fuel-weight variation with t/c has a nearly zero slope at $t/c = 1.5\%$. This occurs because the fuel weight required to meet the range constraint is not influenced only by the aerodynamics. As the wing gets thinner and the wing weight increases, there is a point where the fuel weight penalty associated with the increasing weight of the aircraft becomes as important as the fuel weight benefit from the reduced drag. This point occurs near $t/c = 1.5\%$ when using linear theory analysis. When using Euler analysis, the fuel weight is still dominated by the aerodynamic benefits over the range of t/c investigated.

The decreased inboard LE sweep in the optimal designs from Euler aerodynamics is an interesting occurrence. This is not a result of aerodynamic-structural tradeoffs, but rather it is mainly a result of a compromise between aerodynamic influences. With $b/2$ and s_{LE_i} fixed, there is an increase in the size of the outboard section implicit with any increase in Λ_{LE_i}. The aerodynamic tradeoff (Fig. B2) is between the high inboard sweep desired for improved supersonic performance and the size of the outboard section, which has poor supersonic performance. The nonlinear aerodynamic predictions have a relatively larger fuel weight penalty associated with the outboard section than do the linear theory results. This naturally shifts the optimal Λ_{LE_i} to a lower value.

The wing weight plot in Fig. B2 shows a Λ_{LE_i} compromise between structural effects as well. At the lowest wing sweep, the planform takes on a structurally sound shape. However, the large planform area results in extra weight. At the other extreme, the planform area is reduced, but the design is not as sound structurally. Extra weight is required to strengthen the structure. The best design is a tradeoff between these two influences.

Appendix C: Design of Experiments

Design of experiments theory provides a systematic means of selecting the set of points (called an experimental design) within the m-dimensional design space at which to perform computational analyses. The 2^m vertices formed by the upper and lower bounds on the design variables define the design bounding box or hypercube within which the experimental design is created. The range of each design variable is scaled to span $[-1, 1]$ for both numerical stability and ease of notation.[34] To create the experimental design, the ranges of the design variables are discretized at evenly spaced intervals. For example, a 2^m full factorial design is created by specifying each design variable at two levels: the lower bound (-1) and the upper bound (1). Therefore, this experimental design consists of every vertex in the design bounding box. The type of experimental design created is defined by the number of intervals and the distribution of the points on those intervals. The choice of experimental design depends on the dimension of the problem, the computational resources available, and the type of function to which one wishes to fit the data. Four types of experimental designs are used in this research: 3^m full factorial designs,[35] face-centered central-composite designs,[34,35] small-composite designs,[34] and D-optimal experimental designs.[31]

A 3^m full factorial design[35] is created by specifying the design variables at three levels $(-1, 0, 1)$ corresponding to the

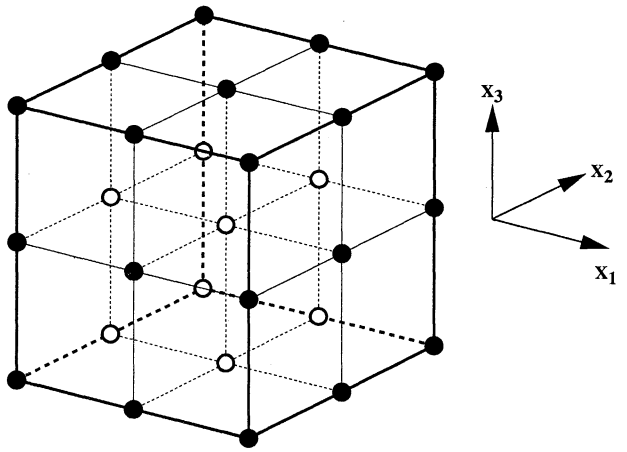

Fig. C1 3^3 full factorial experimental design.

lower bound, midpoint, and upper bound of the design variables. A 3^3 experimental design is presented in Fig. C1. This experimental design provides sufficient information to construct quadratic polynomial RS models. However, as the number of design variables increases, the number of computational experiments required becomes prohibitively large. For example, a 3^m full factorial design in a 20-dimensional space requires $3^{20} \approx 3.5 \times 10^9$ computational experiments.

A face-centered central-composite design[34,35] enables resolution of quadratic terms in the RS models with fewer computational experiments. It is created by taking a 2^m full factorial design and adding 2^m star points on the faces of the hypercube and another point in the middle of the design hypercube. The star points correspond to a set of design variables in which all variables are held at their midpoint value except for a single variable that is specified at either its upper or lower bound. As the number of design variables is increased, these experimental designs also become prohibitively large. Creating a face-centered central-composite design in a 20-dimensional space requires $2^{20} + 2 \times 20 + 1 \approx 1.0 \times 10^6$ computational experiments.

The small-composite experimental design[34] allows even fewer computational experiments with which to evaluate quadratic RS models. This experimental design is constructed in a manner similar to that for the central-composite design, except that a fractional factorial[34] experimental design is used in place of the 2^m full factorial design. The fractional factorial design includes only $2^{m-\beta}$ vertices of the m-dimensional bounding box (β is an integer number smaller than m). There is some freedom in the value of β; however, it cannot be too large or there will be insufficient data to properly resolve all terms in the quadratic polynomial. Certain vertices of the design space will not have any associated data when using this experimental design. While this is not an ideal situation, it is inevitable because the number of vertices grows exponentially with the number of design variables.

The final experimental design used in this study is the D-optimal experimental design.[31] Using D-optimal designs allows a flexibility in the number of computational experiments that is not allowed in the classical experimental designs. D-optimal designs are also well suited for irregularly shaped design spaces, while the classical designs are best suited to rectangular design spaces. D-optimal designs minimize the uncertainty in the polynomial coefficient estimates and in the predicted value of the response. To create a D-optimal experimental design, one selects p design points out of q candidate points. In this research, the candidate points are derived from one of the three classical experimental designs described earlier. An iterative optimization method is then used to find the p D-optimal points.

For the 5- and 10-variable cases, the JMP[32] statistical software package is used to provide the D-optimal designs. The approach implemented in JMP uses sets of randomly selected seed candidate points from the classical design, and the best points in terms of the prediction variance are kept throughout the iterative procedure. Because the design points are selected in a quasirandom manner, it is unlikely that the experimental design chosen from JMP is truly a D-optimal set. Limitations in JMP prevent its use for the larger design problems. A routine employing Mitchell's k-exchange method,[36] developed by Dan Haim, is used for the 15- and 20-variable cases.

Acknowledgments

Support for this research was provided through NASA Langley Research Center Grants NAG1-1160 with Peter Coen as Contract Monitor, and NAG1-1562 with Perry Newman as Contract Monitor.

References

[1]Giesing, J. P., Agrawal, S., and Bharadvaj, B. K., "The Role of Computational Fluid Dynamics in Multidisciplinary Design Optimization of Transport Aircraft," *Proceedings of the 6th International Symposium on Computational Fluid Dynamics, Technology, and Operations Congress* (Lake Tahoe, CA), 1995.

[2]Nicolai, L. M., *Fundamentals of Aircraft Design*, E. P. Domicone Printing Services, Fairborne, OH, 1975, pp. 24·23–24·25.

[3]Hutchison, M. G., Unger, E. R., Mason, W. H., Grossman, B., and Haftka, R. T., "Variable-Complexity Aerodynamic Optimization of a High-Speed Civil Transport Wing," *Journal of Aircraft*, Vol. 31, No. 1, 1994, pp. 110–116.

[4]Giunta, A. A., Narducci, R., Burgee, S., Grossman, B., Mason, W. H., Watson, L. T., and Haftka, R. T., "Variable-Complexity Response Surface Aerodynamic Design of an HSCT Wing," AIAA Paper 95-1886, June 1995.

[5]Kaufman, M., Balabanov, V., Burgee, S. L., Giunta, A. A., Grossman, B., Haftka, R. T., Mason, W. H., and Watson, L. T., "Variable-Complexity Response Surface Approximations for Wing Structural Weight in HSCT Design." *Journal of Computational Mechanics*, Vol. 18, No. 2, 1996, pp. 112–126.

[6]Balabanov, V., Kaufman, M., Knill, D. L., Haim, D., Golovidov, O., Giunta, A. A., Haftka, R. T., Grossman, B., Mason, W. H., and Watson, L. T., "Dependence of Optimal Structural Weight on Aerodynamic Shape for a High-Speed Civil Transport," AIAA Paper 96-4046, Sept. 1996.

[7]Burgee, S., Giunta, A. A., Balabanov, V., Grossman, B., Mason, W. H., Narducci, R., Haftka, R. T., and Watson, L. T., "A Coarse Grained Parallel Variable-Complexity Multidisciplinary Optimization Paradigm," *International Journal of Supercomputing Applications and High Performance Computing*, Vol. 10, No. 4, 1996, pp. 269–299.

[8]Eminton, E., "On the Minimization and Numerical Evaluation of Wave Drag," Royal Aircraft Establishment, Rep. AERO.2564, Nov. 1955.

[9]Harris, R. V., Jr., "An Analysis and Correlation of Aircraft Wave Drag," NASA TM X-947, March 1964.

[10]Carlson, H. W., and Miller, D. S., "Numerical Methods for the Design and Analysis of Wings at Supersonic Speeds," NASA TN D-7713, Dec. 1974.

[11]Carlson, H. W., and Mack, R. J., "Estimation of Leading-Edge Thrust for Supersonic Wings of Arbitrary Planforms," NASA TP-1270, Oct. 1978.

[12]Hopkins, E. J., "Charts for Predicting Turbulent Skin Friction from the van Driest Method (II)," NASA TN D-6945, Oct. 1972.

[13]Carlson, H. W., and Walkley, K. B., "Numerical Methods and a Computer Program for Subsonic and Supersonic Aerodynamic Design and Analysis of Wings with Attainable Thrust Corrections," NASA CR-3808, Aug. 1984.

[14]McGrory, W. D., Slack, D. C., Applebaum, M. P., and Walters, R. W., *GASP Version 2.2 Users Manual*, Aerosoft, Inc., Blacksburg, VA, 1993.

[15]Knill, D. L., Balabanov, V., Golovidov, O., Grossman, B., Mason, W. H., Haftka, R. T., and Watson, L. T., "Accuracy of Aerodynamic Predictions and Its Effects on Supersonic Transport Design," Multidisciplinary Analysis and Design Center for Advanced Vehicles, Virginia Polytechnic Inst. and State Univ., Rept. 96-12-01, Blacksburg, VA, Dec. 1996.

[16]Barger, R. L., Adams, M. S., and Krishnan, R. R., "Automatic Computation of Euler-Marching and Subsonic Grids for Wing-Fuselage Configurations," NASA TM 4573, July 1994.

[17]Knill, D. L., "Implementing Aerodynamic Predictions from Computational Fluid Dynamics in Multidisciplinary Design Optimization of a High-Speed Civil Transport," Ph.D. Dissertation, Dept. of Aerospace and Ocean Engineering, Virginia Polytechnic Inst. and State Univ., Blacksburg, VA, Dec. 1997; also in Multidisciplinary Analysis and Design Center for Advanced Vehicles, Rept. 97-12-01, Dec. 1997.

[18]Craidon, C. B., "Description of a Digital Computer Program for Airplane Configuration Plots," NASA TM X-2074, Sept. 1970.

[19]Barger, R. L., and Adams, M. S., "Automatic Computation of Wing-Fuselage Intersection Lines and Fillet Inserts with Fixed-Area Constraint," NASA TM 4406, March 1993.

[20]McCullers, L. A., "Aircraft Configuration Optimization Including Optimized Flight Profiles," *Proceedings of the Symposium on Recent Experiences in Multidisciplinary Analysis and Optimization*, compiled by J. Sobieski, 1984, pp. 396–412 (NASA CP-2327).

[21]*DOT Users Manual, Version 4.20*, Vanderplaats Research & Development, Inc., Colorado Springs, CO, 1995.

[22]Powers, S. A., "Drag Minimization Using Exact Methods," *AIAA Journal*, Vol. 2, No. 5, 1964, pp. 941–943.

[23]Giunta, A. A., Balabanov, V., Haim, D., Grossman, B., Mason, W. H., Watson, L. T., and Haftka, R. T., "Multidisciplinary Optimisation of a Supersonic Transport Using Design of Experiments Theory and Response Surface Modelling," *The Aeronautical Journal of the Royal Aeronautical Society*, Vol. 101, No. 1008, 1997, 347–356.

[24]Sellar, R. S., Stelmack, M. A., Batill, S. M., and Renaud, J. E., "Response Surface Approximations for Discipline Coordination in Multidisciplinary Design Optimization," AIAA Paper 96-1383, April 1996.

[25]Chen, W., Allen, J. K., Schrage, D. P., and Mistree, F., "Statistical Experimentation Methods for Achieving Affordable Concurrent Systems Design," *AIAA Journal*, Vol. 35, No. 5, 1997, pp. 893–900.

[26]Giunta, A. A., Balabanov, V., Haim, D., Grossman, B., Mason, W. H., Watson, L. T., and Haftka, R. T., "Wing Design for a High-Speed Civil Transport Using a Design of Experiments Methodology," AIAA Paper 96-4001, Sept. 1996.

[27]Venter, G., Haftka, R. T., and Starnes, J. H., "Construction of Response Surfaces for Design Optimization Applications," AIAA Paper 96-4040, Sept. 1996.

[28]Haftka, R. T., and Gürdal, Z., *Elements of Structural Optimization*, 3rd ed., Kluwer, Dordrecht, The Netherlands, 1992, pp. 211–219.

[29]Golovidov, O., "Variable-Complexity Response Surface Approximations for Aerodynamic Parameters in HSCT Optimization," Multidisciplinary Analysis and Design Center for Advanced Vehicles, Virginia Polytechnic Inst. and State Univ., Rept. 97-06-01, Blacksburg, VA, June 1997.

[30]Giunta, A. A., Dudley, J. M., Narducci, R., Grossman, B., Haftka, R. T., Mason, W. H., and Watson, L. T., "Noisy Aerodynamic Response and Smooth Approximations in HSCT Design," AIAA Paper 94-4376, Sept. 1994.

[31]Box, M. H., and Draper, N. R., "Factorial Designs, the $|X^TX|$ Criterion, and Some Related Matters," *Technometrics*, Vol. 13, No. 4, 1971, pp. 731–742.

[32]*JMP Users Guide, Version 3.1*, SAS Inst., Inc., Cary, NC, 1995.

[33]Knill, D. L., Giunta, A. A., Baker, C. A., Grossman, B., Mason, W. H., Haftka, R. T., and Watson, L. T., "Multidisciplinary HSCT Design Using Response Surface Approximations of Supersonic Euler Aerodynamics," AIAA Paper 98-0905, Jan. 1998.

[34]Myers, R. H., and Montgomery, D. C., *Response Surface Methodology: Process and Product Optimization Using Designed Experiments*, Wiley, New York, 1995, pp. 1–67, 134–174, 297–357, 640–655.

[35]Mead, R., *The Design of Experiments*, Cambridge Univ. Press, New York, 1988, pp. 542–548.

[36]Mitchell, T. J., "An Algorithm for the Construction of *D*-Optimal Experimental Designs," *Technometrics*, Vol. 16, No. 2, 1974, pp. 203–210.